Magnetoelastic properties of multiferroic hexagonal ErMnO$_3$

C.M. Fernandez-Posada[a], C.R.S. Haines[a], D.M. Evans[b], Z. Yan[c], E. Bourret[d], D. Meier[b], M.A. Carpenter[a]

[a] *Department of Earth Sciences, University of Cambridge, Downing Street, Cambridge CB2 3EQ, UK.*
[b] *Department of Materials Science and Engineering, Norwegian University of Science and Technology, NTNU, 7043 Trondheim, Norway*
[c] *Department of Physics, ETH Zurich, Otto-Stern-Weg 1, 8093 Zurich, Switzerland*
[d] *Materials Sciences Division, Lawrence Berkeley National Laboratory, Berkeley, California 94720,USA*

ARTICLE INFO

ABSTRACT

The strength and dynamics of magnetoelastic coupling through the paramagnetic (PM) – antiferromagnetic (AFM) – ferrimagnetic (FIM) transitions in multiferroic hexagonal ErMnO$_3$ have been investigated by Resonant Ultrasound Spectroscopy. Elastic stiffening by up to 2% below the PM – AFM transition at 80 K arises from biquadratic coupling between strain and the magnetic order parameter with relaxation times longer than ~10^{-6} s for the response of spins to changes in strain. In contrast with YMnO$_3$, the PM – AFM transition in ErMnO$_3$ is accompanied by a peak in acoustic loss immediately below the Néel point which is interpreted in terms of strain relaxation accompanying ordering of spins of Er^{3+} at 4b sites. Changes in the magnetic ordering scheme at the AFM – FIM transition near 3 K are accompanied by elastic softening of ~0.03 %. Poling of the low temperature ferrimagnetic structure round magnetic hysteresis loops is detected as small changes in elastic stiffness which arise due to the contribution of piezomagnetic and/or piezoelectric moduli. Contributions of piezoelectric moduli to acoustic resonance frequencies also permit changes in the configuration of ferroelectric domains to be detected in response both to cycling through this transition and to application of a magnetic field. A peak in acoustic loss in the vicinity of 250 K is attributed to strain-mediated pinning/freezing of some aspect of the domain microstructure with an activation energy of ~0.25-0.3 eV. A return to the original elastic properties on heating to temperatures above ~250 K is interpreted in terms of backswitching of domains to the configuration they had at the start. These observations confirm the existence of subtle variations in magnetoelastic coupling behaviour relating to both the magnetic order parameters and magnetic domain structures.

1. Introduction

Members of the family of multiferroic hexagonal manganites, RMnO$_3$ (R = Sc, Y, In, Dy-Lu), are ferroelectric due to a structural phase transition within the interval ~1000-1500 K [1-5] and antiferromagnetic due to a magnetic ordering transition within the interval ~60-130 K [6-10]. Their structures at high temperatures and at room temperature are in space groups $P6_3/mmc$ and $P6_3cm$, respectively [3,5,10-13]. The structural transition $P6_3/mmc \rightarrow P6_3cm$ includes a geometrical tilt that displaces charged atoms in the structure, resulting in spontaneous polarization oriented along the crystallographic c-axis and making it improper ferroelectric [5,12,14,15]. Antiferromagnetic (AFM) ordering within the ferroelectric structure is driven by interactions between individual moments at Mn^{3+} sites. In the hexagonal RMnO$_3$ phases where ordering of moments at the R^{3+} cation sites is also possible, further magnetic transitions occur at much lower temperatures that are typically below a few degrees K (e.g. refs. 8,16,17). Ordering of R^{3+} moments influences the stable AFM configuration of Mn^{3+} moments and, as a result, leads to a rich diversity of equilibrium phase relationships with respect to variations in temperature and magnetic field [7-9,18-22].

A central theme of the extensive interest in these phases relates to the properties of different domain structures which develop as a consequence of the structural and magnetic phase transitions. As set out, for example, in refs. [15,23-29]: (a) the structural transition results in a microstructure of antiphase domains which, when combined with different possible orientations of the electric dipole, leads to a total of six different domains, (b) the domains meet in groups of six to create vortices, and (c) some of the domain walls have bound charges that require electrical screening, while others are neutral. It has been demonstrated, further, that some domain walls are electrically conducting (e.g. refs. [30-34]). Below the Néel point of each phase, a microstructure of AFM domains becomes superimposed on the microstructure of structural/ferroelectric domains

inherited from higher temperatures. Direct observation of these in YMnO$_3$ and ErMnO$_3$ has shown that the two types of domain walls can couple [35-40]. In YMnO$_3$, ferroelectric domain walls also demarcate boundaries between AFM domains whereas AFM domain walls can exist separately within individual ferroelectric domains without a change in orientation of electric polarisation [35]. Additional magnetic transitions at the lowest temperatures due to ordering of moments at the R^{3+} cation must result in the development of further sets of domains.

Possibilities for taking advantage of the multiferroic properties of hexagonal manganites in device applications, whether as bulk samples or thin films, depend on the potential for engineering microstructures with chosen and favourable distributions of domain walls. If the device requires long term stability involving strongly localised electrical conductivity, say, the domain walls may need to be strongly pinned. On the other hand, if the requirement is for fast switching, the domain walls must remain mobile in response to an external field. In this context, a characteristic and completely general mechanism for pinning of domain walls is via interacting strain fields at point defects. This is additional to the pervasive role of strain at almost all structural, ferroelectric and magnetic phase transitions in promoting mean field behaviour, in providing a mechanism for coupling between multiple order parameters and in generating local strain fields within and across individual domain boundaries. Acoustic spectroscopy provides the most straightforward approach for investigating static and dynamic strain relaxation behaviour through the variations of elastic and anelastic properties, as summarised elsewhere for a wide variety of ferroic perovskites using Resonant Ultrasound Spectroscopy (RUS) [41].

The present study follows from recent work on strain relaxation in multiferroic orthorhombic manganites, where the initial structural transition is ferroelastic [42]. Coupling of strain with the ferroelectric and magnetic order parameters in orthorhombic GdMnO$_3$, TbMnO$_3$ and Sm$_{0.6}$Y$_{0.4}$MnO$_3$ is weak but the existence of acoustic loss peaks provides evidence of

Debye-like freezing processes involving local, dynamic correlations of electric and magnetic polarisation ahead of the stability fields of the multiferroic structures. The same methodology has been adopted here to investigate the magnetoelastic properties of $ErMnO_3$ as a representative of hexagonal manganites with magnetic R^{3+} cations, to be compared with a previous study of $YMnO_3$ as being representative of hexagonal manganites in which the R^{3+} cation is non-magnetic.

The first a priori aspect of strain relaxation behaviour in $ErMnO_3$ and $YMnO_3$, is that the structural transition is coelastic, rather than ferroelastic, i.e. it is not accompanied by a symmetry breaking shear strain. As a consequence, individual structural/ferroelectric domain walls are not expected to move in response to an externally applied shear stress. Wang et al. [43] have shown that shear stress applied at high temperatures can induce movement of vortices where the domain walls meet but the conditions which apply in the RUS experiments presented here, both in terms of load and temperature, are far below those applied by Wang et al. [43]. Secondly, the elastic modulus matrix has the same form for both crystallographic point group 6/mmm ($P6_3/mmc$ structure) and crystallographic point group 6mm ($P6_3cm$ structure). This means that elastic moduli measured from a single crystal should be independent of the distribution and proportion of multiple domain orientations that it contains. Thirdly, the ferroelectric structure is also piezoelectric and the magnetic structures are piezomagnetic. Net piezoelectric/piezomagnetic moduli measured for a crystal with equal proportions of all possible domains will be zero but will become non-zero if the distribution of orientations becomes unequal. Since acoustic resonance frequencies of the whole crystal depend on both the elastic and piezo moduli, changes in domain configurations in response to changes in temperature and magnetic field should be detectable as small changes of resonance frequencies.

The primary objective of this study was to determine the dynamical magnetoelastic properties of $ErMnO_3$, as a representative of hexagonal manganite perovskites. New data obtained by Resonant Ultrasound Spectroscopy reveal subtle variations in elastic properties of $ErMnO_3$ which are sensitive to changes in domain configurations, such as around a magnetic hysteresis loop. Hysteretic responses to changing temperature and small discontinuities in response to increasing magnetic field are attributed to jerky motion of both magnetic and ferroelectric domain walls between pinning positions. The influence of triggered ordering of moments at Er^{3+} on 4b sites appears to be a peak in acoustic loss immediately below the Néel point, while additional ordering of moments at 2a sites leads to small changes in bulk elastic properties below ~3 K. These results confirm that, as in orthorhombic multiferroic manganites, strain coupling has a small but significant role in determining both static and dynamic physical properties.

2. Relationship between ferroelectric and magnetic structures of $ErMnO_3$

Figure 1 shows the phase relationships given in Figure 2 of Meier et al. [44] for the different magnetic structures of $ErMnO_3$. The paramagnetic structure, PM, is in space group $P6_3cm$ and the AFM structure orders according to magnetic space group $P6_3'c'm$, with a second transition to $P6_3c'm'$ at low temperature. In zero field these two transitions are marked by distinct anomalies in heat capacity at ~80 and ~2.5 K [7,45-48. Meier et al. [44] showed the PM → AFM transition as being driven by ordering of moments at Mn^{3+} in directions lying within (001) planes, triggering antiferromagnetic ordering of moments at Er^{3+} parallel and antiparallel to [001] on 4b sites ($P6_3'c'm$). Er^{3+} moments on the 2a sites then order below 10 K, inducing a reorientation of Mn^{3+} moments and the Er^{3+} moments at 4b sites,

to give a structure with magnetic space group $P6_3c'm'$. In this structure the Mn^{3+} moments have a different orientation within the (001) plane but maintain their antiferromagnetic alignment. Moments at Er^{3+} on 4b sites are aligned parallel to [001] and moments at Er^{3+} on 2a sites are aligned in the opposite direction to give a net ferrimagnetic moment (FIM_1). Application of a magnetic field with $H//c$ leads to a single-domain state of the ferrimagnetic structure, $FIM_1 \rightarrow FIM_2$. At sufficiently large magnetic fields, a field-aligned ferromagnetic (FM) structure develops, also in space group $P6_3c'm'$ but with all moments at Er^{3+} aligned parallel to [001].
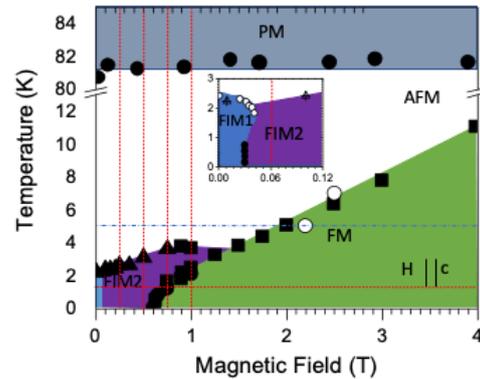
Fig. 1. Magnetic phase diagram of hexagonal $ErMnO_3$ for fields applied parallel to the crystallographic c-axis ($H//c$), adapted from [44]. PM = paramagnetic), FM = ferromagnetic (field aligned), FIM_1 = ferrimagnetic (multidomain), FIM_2 = ferrimagnetic (single domain state). Crystal 1 of the present study was the same crystal as used by Meier et al. [44] to determine boundaries between the stability fields of the magnetic structures. Discontinuous red lines mark the loci of temperature sweeps at constant magnetic field strength and magnetic field sweeps at constant temperature applied in RUS experiments described below. The blue dot-dash line marks the temperature/field trajectory applied to Crystal 2, though the field was not applied parallel to [001] in this case.

In the present study, elasticity measurements were made on two different floating-zone grown single crystals of $ErMnO_3$ and one of $Er_{0.99}Zr_{0.01}MnO_3$. The first $ErMnO_3$ crystal (Crystal 1) was the same one as had been used to determine the boundaries between AFM, FIM and FM structures in Figure 1, based on neutron diffraction and magnetic measurements [44]. The second crystal (Crystal 2) is from the same batch as used in refs. [39,49]. Both have a Néel temperature in zero field of $T_N = 80$ K, but are likely to differ in oxygen stoichiometry as they originate from different batches. Red dotted lines show the trajectories used for RUS measurements on this crystal as a function of temperature at constant applied field and as a function of field at constant temperature. The blue dash-dot line shows the trajectory of one set of measurements on the second crystal though, in this case, the orientation of the crystallographic axes with respect to the applied field was not known.

3. Materials and methods

All three crystals used for this study had an irregular acicular shape with maximum dimensions of ~3, ~1 and ~0.5 mm in orthogonal directions. The long dimension of the first crystal of $ErMnO_3$ (Crystal 1) was aligned parallel to [001] and had mass ~20 mg at the start. Part way through the RUS experiments this crystal broke into two pieces, the larger of which had mass 12.4 mg and was used for subsequent measurements. The second $ErMnO_3$ crystal (Crystal 2) had mass 16.3 mg; crystallographic orientations were not further specified prior to the RUS measurements. The Zr-doped crystal had mass 21.9 mg and came from the same boule as the sample used in the work of Holstad et al. [49].

A complete description of the RUS technique has been given by Migliori and Sarrao [50]. The sample can have a regular or

irregular shape with dimensions in the range ~1-5 mm and is held between two piezoelectric transducers, one of which is used to excite acoustic resonances and the other to detect them. In the Cambridge set-up [51,52] the sample holder is lowered into an Oxford Instruments Teslatron cryostat which has a superconducting magnet capable of applying a field of up to 14 T. He gas is used to assist thermal equilibration between the sample and the walls of the sample chamber. Spectra are obtained in automated sequences which include a dwell time at each set point before the onset of data collection. Absolute values of the temperature of the sample at each set point are believed to be known to better than ± 1 K, based on the experience of studying phase transitions in many different materials. The temperature resolution of the instrument is better than ± 0.1 K, but this does not represent an absolute uncertainty for the temperature of the sample. The maximum voltage applied to the driving transducer is typically 2 V.

Measurements with the magnet turned on were made on Crystal 1 with its long axis perpendicular to the faces of the transducers and parallel to the field, i.e. $H//c$. In an additional set of measurements in zero field, the crystal was held with its long axis parallel to the faces of the transducers. The other two crystals had their largest faces resting between the transducers, i.e. with their long axes perpendicular to the direction of the field.

A preliminary cooling/heating sequence on Crystal 1 was in 5 K steps between room temperature and ~10 K. Each spectrum contained 65,000 data points in the frequency range 0.01-1.2 MHz, and the dwell time was 15 minutes. For sequences with smaller steps the temperature interval was between ~2 and 100 K. For temperature sweeps in constant field ($H//c$), the frequency range was 0.01-1.2, 0.2-1.2 or 0.4-1.2 MHz and the number of data points was 130,000 per spectrum. For magnetic field sweeps ($H//c$) at fixed temperatures the frequency range was 0.4-1.2 MHz with 130,000 data points per spectrum and a dwell time of 10 minutes. Initially the crystal had mass 20 mg but it broke into two pieces during one of the field sweeps. The larger of these, with mass 12.4 g, was used for subsequent sequences.

For measurements with the long direction of Crystal 1 parallel to the faces of the transducers, spectra were collected in zero field between room temperature and 1.5 or 1.7 K, using steps of 0.1 or 0.2 K below 5 K. The frequency range was 0.1-1.2 MHz or 0.3-1.9 MHz, with 130,000 data points per spectrum and a dwell time of 20 minutes. In the final set of repeat measurements, with the long axis of the 12.4 mg piece held with its long axis parallel to the faces of the transducers, the sample chamber was filled with 1 bar He at room temperature, rather than just a few mbars as had been used previously.

Spectra were collected from Crystal 2 and the Zr-doped crystal as a function of temperature in zero field with 5 K steps between 295 and 5 K. Each spectrum contained 65,000 data points in the frequency range 0.1-1.2 MHz. The dwell time for thermal equilibration at each set point was 15 minutes. Spectra collected from Crystal 2 as a function of increasing magnetic field at 5 K had the same resolution and frequency range, and a dwell time of 10 minutes.

An asymmetric Lorentzian function was used in the software package IGOR (WaveMetrics) to determine values of the peak frequency, f, and width at half maximum height, Δf, of selected resonance peaks. Values of f^2 scale with values of the different combinations of elastic moduli for the distortions involved in each resonance. Most resonances involve predominantly shearing motions, with relatively small contributions from breathing, so that the main variations observed are of combinations of shear elastic moduli. Acoustic attenuation is expressed in terms of the inverse mechanical quality factor, Q^{-1}, which is treated here as being given by $\Delta f/f$.

4. Results

4.1 ErMnO₃ Crystal 1 in zero field

Figure 2 provides an overview of the variations of f^2 and Q^{-1} for resonance peaks observed to have frequencies in the range ~0.3-2 MHz during heating from 1.5 to 300 K, measured when the long axis of the 12.4 mg crystal was lying parallel to the faces of the transducer. Peaks with frequencies greater than ~850 kHz show marked stiffening (increasing values of f^2) below 80 K and a rounded peak in Q^{-1} with its maximum at or just below the temperature at which the break in slope occurs. The degree of stiffening varies between resonances, up to a maximum of ~1.5%, and those with the largest variation also show softening as the Néel point was approached from above (Fig. 2a). Some of the resonances, such as at ~1070 kHz, show a slight additional stiffening below ~30-40 K. Resonances with the lowest frequencies, ~350–800 kHz, show almost no anomaly in either f^2 or Q^{-1} at ~80 K but reveal an additional softening with falling temperature below ~20 K (Fig. 2b). All the resonances display a general increase in Q^{-1} with increasing temperature and a rounded maximum at ~250–270 K. Some precursor variations in f^2 occurred with falling temperature below ~6-10 K, followed by a small step-like softening of ~0.03% below ~3 K (Fig. 2c). There are no systematic anomalies in Q^{-1} from any resonances at these lowest temperatures.
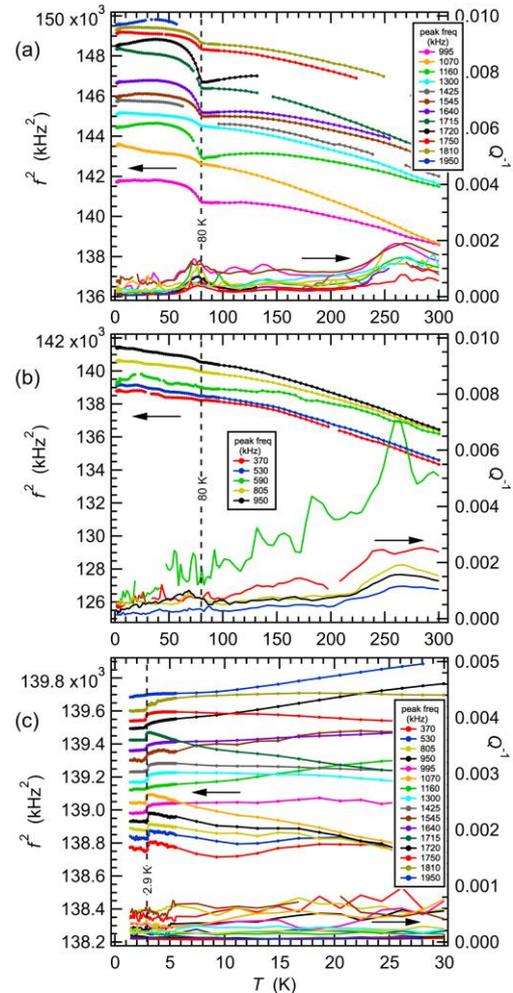
Fig. 2. f^2 and Q^{-1} variations from spectra collected using the 12.4 mg piece of Crystal 1 in a continuous heating cycle from 1.5 to 300 K. Frequencies listed in the text boxes refer to the approximate frequency of each resonance peak at room temperature. Absolute values of f^2 have been rescaled by arbitrary factors along the y-axis in order to allow easy comparison of their temperature dependences. Gaps in the data are where resonance peaks in the primary spectra could not be fit due to noise, peak overlaps or low intensities. (a) Data for resonances with frequencies in the range ~1–2 MHz: stiffening below 80 K, rounded maxima in Q^{-1} at ~250-270 K and at ~75-80 K. (b) Data for

resonances with frequencies in the range ~300–900 kHz: smaller degree of stiffening below 80 K and weaker anomaly in Q^{-1} at ~75-80 K. (c) $T < 30K$: most resonances show small, abrupt softening below ~3 K (marked here by a vertical line at 2.9 K) and some show precursor softening below ~6 K, ahead of the AFM – FIM_1 transition. Resonances with the lowest frequencies have a pattern of softening between ~20 and 10 K followed by stiffening down to ~5 K.

Stepwise softening seen below ~3 K for all the resonances in Figure 2c correlates with the small heat capacity anomaly that marks the discrete AFM – FIM_1 phase transition at ~2.0–2.5 K in zero field [7,44,45]. The smaller precursor elastic softening below ~6 K also correlates with a dip in the intensity of a magnetic ordering reflection in neutron diffraction patterns shown in Figure 6a of Meier et al. [44]. Thus there are clearly elastic responses associated with the sequence of magnetic ordering reported by Meier et al. [44] involving ordering of moments at Er^{3+} on 2a sites below ~10 K, reorientation of ordered moments of Er^{3+} at 4b sites below ~7 K and reorientation of moments at Mn^{3+} at the transition point itself (2.5 K) [44]. Figure 3 has data collected at intervals of 0.1 K which reveal additional subtle details of the transition that have not yet been characterised by other methods. These include hysteresis which is the wrong way round for a classical first order transition which would normally be expected to occur at a higher temperature during heating than during cooling. Instrumental factors relating to temperature control cannot be entirely ruled out at these fine temperature intervals, but would not account for differences between the evolution of the two resonances shown. One possibility is that microstructures associated with the magnetic ordering transitions do not evolve in the same way between cooling and heating.
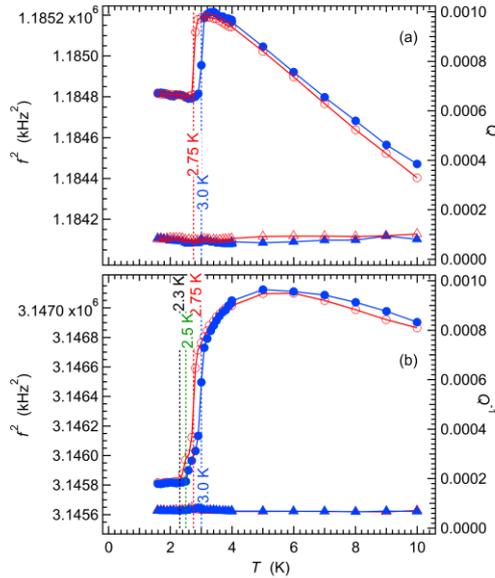
Fig. 3. Details of f^2 (open and filled circles) and Q^{-1} (open and filled triangles) variations for two representative resonance peaks in spectra collected during cooling (blue filled symbols), followed by heating (red open symbols), between 10 and 1.7 K. Crystal 1 (12.4 mg), long axis parallel to the faces of the transducers. (a) Resonance with frequency near 1089 kHz: a step like change in f^2 occurred at 3.0 K during cooling and at 2.75 K during heating. (b) Resonance with frequency near 1774 kHz: precursor softening occurred below ~5 K. In addition to the steep changes at 3.0 and 2.75 K, there are less steep changes which reached approximately constant values at 2.5 K (cooling) and 2.3 K (heating).

Details of three representative resonances in spectra collected in an early cycle between 100 and 2 K are shown in Figure 4. The sharp break in slope of f^2 during both heating and cooling is at ~80 K, and the peak in Q^{-1} occurs at ~75 K. Maximum values of Q^{-1}, up to ~0.001, and the amount of stiffening below T_N differ between resonances and, therefore, between different combinations of single crystal elastic moduli.

There is a distinct hysteresis between the evolution f^2 as functions of decreasing and increasing temperature. Higher values developed during heating, with ~30 K as the temperature at which the divergence began. As discussed in section 5.3, below, this is likely to have been due to differences in the configuration of ferroelectric domains between heating and cooling.

Typical patterns of variations of elastic moduli through a phase transition depend on coupling of the order parameter, m, with strain, e. Lowest order coupling terms have the form $\lambda e m^2$ for the spontaneous strains e_1 and e_3 of hexagonal manganites [53]. These would be expected to give rise to softening of the elastic moduli below T_N with similar form to that seen for the model system CoF_2 [54]. However, as discussed for $YMnO_3$ [53], if the magnetic order parameter does not relax on the time scale of the dynamical strain in an acoustic resonance, the elastic response is determined by the next higher order terms which have the form $\lambda e^2 m^2$. Stiffening or softening, depending on the sign of the coupling coefficient λ, then occurs in proportion to m^2. Stiffening of resonances with frequencies greater than ~900 kHz from $ErMnO_3$ has a form similar to the variation of m^2 indicated by the intensity $I (\propto m^2)$ of superlattice reflections in neutron diffraction patterns (Figs. 3a,e of ref. [44]). Resonances with lower frequencies (elastically softer) did not show the same stiffening, suggesting that values of the coupling coefficients are smallest for strains that form part of the shear modes with the smallest effective elastic moduli.
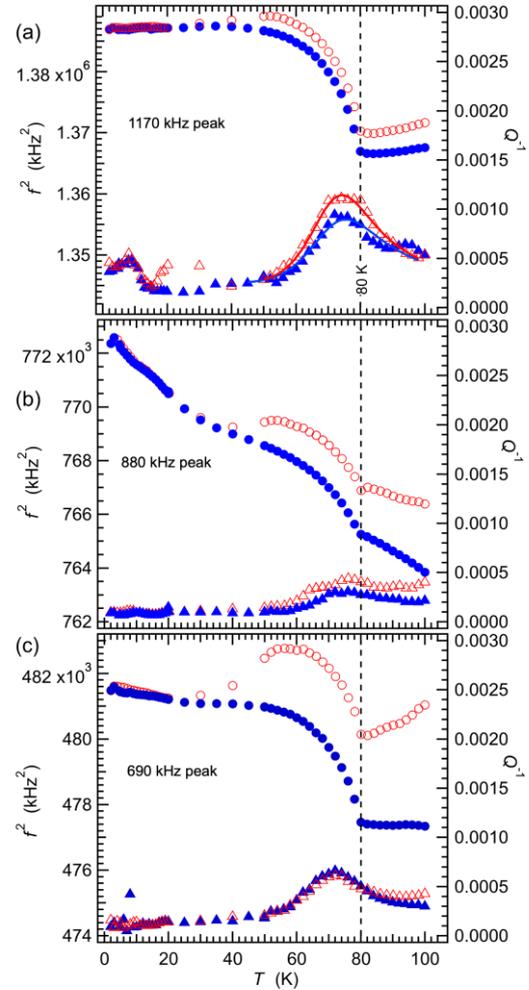
Fig. 4. Details of f^2 (open and filled circles) and Q^{-1} (open and filled triangles) variations for three representative resonance peaks in spectra collected during cooling (blue filled symbols), followed by heating (red open symbols), between 100 and 2 K from Crystal 1 (20 mg). The long axis was aligned perpendicular to the faces of the transducers. (a) The resonance near 1170 kHz shows the largest degree of stiffening (~1.5%) below T_N and the largest peak

in Q^{-1} at ~75 K. An additional anomaly in Q^{-1} at ~9 K does not appear in data extracted from other resonance peaks and is considered to be an artefact. Solid curves are fits of Equation 1 to the data for Q^{-1}: $E_a/Rr_2(\beta)$ = 595 ± 13 K, T_m = 74.3 ± 0.2 K, Q_m^{-1} = 0.00089 ± 0.00001 (heating); $E_a/Rr_2(\beta)$ = 550 ± 33 K, T_m = 75.4 ± 0.5 K, Q_m^{-1} = 0.00065 ± 0.00003 (cooling). (b) Resonance with frequency near 860 kHz. This is representative of lower frequency resonances which showed the smallest change in trend of f^2 below ~80 K and the smallest peak Q^{-1} at ~75 K. (c) Resonance peak near 690 kHz. This displays most clearly the differences in f^2 values between cooling and heating at temperatures above ~30 K.

Q^{-1} data for ErMnO$_3$ have a rounded peak a few degrees below T_N (Fig. 4a,c), which is in direct contrast with YMnO$_3$ which did not give any anomaly in Q^{-1} at the AFM transition [53]. This also differs from the AFM ordering transition in CoF$_2$, where the loss has a sharp maximum at T_N and has been interpreted in terms of critical slowing down [54]. If, instead, the loss mechanism involves some thermally activated pinning or freezing process, a Debye-like description such as given by [55] might apply:

$$Q^{-1}(T) = Q_m^{-1}\left[\cosh\left\{\frac{E_a}{Rr_2(\beta)}\left(\frac{1}{T}-\frac{1}{T_m}\right)\right\}\right]^{-1}. \qquad (1)$$

T_m is the temperature at which the maximum value of Q^{-1}, Q_m^{-1}, occurs, and the value of Q_m^{-1} is related to the difference in elastic moduli between relaxed and unrelaxed states. T is temperature and R is the gas constant. The width of the peak in Q^{-1} depends on the activation energy, E_a, and the parameter $r_2(\beta)$. The value of $r_2(\beta)$ is 1 when the dissipation process involves a single relaxation time and greater than 1 if there is a spread of relaxation times. Fits of Equation 1 to the Q^{-1} data from the resonance peak with frequency near 1170 kHz are shown in Figure 4a, and values of the fit parameters are given in the caption. The fits provide an estimate of ~0.05 eV for E_a if $r_2(\beta)$ = 1 and greater than this if $r_2(\beta)$ > 1. A defect pinning or freezing process gives a peak in Q^{-1} at $\omega\tau$ = 1, where τ is relaxation time and ω (= $2\pi f$) is the angular measuring frequency. Classical Arrhenius behaviour is expected to follow $\tau = \tau_0\exp(E_a/RT)$ which, using f = 1170 kHz, E_a = 0.051 eV, T_m = 74.3 K, gives τ_0 = 4.5 x 10^{-11} s.

The peak in Q^{-1} near 250 K is typical of a Debye loss process, and was present in data from every resonance followed in a second data collection (Fig. 5a). Fits of Equation 1 gave E_a = 0.31 ± 0.05 eV for $r_2(\beta)$ = 1. A limitation of the RUS method is the relatively narrow range of frequencies that can be explored but values of T_m from the fits were sufficiently systematic that it has been possible to plot them in Arrhenius form to give E_a = 0.28 ± 0.06 eV (Fig. 5b). Overlap of this value with the value from fitting Equation 1 confirms that the value of $r_2(\beta)$ is close to 1. The intercept yielded $\ln\omega_0$ (= $\ln(1/\tau_0)$) = 28.3 ± 2.6 and, hence, τ_0 between ~7 x 10^{-12} and ~4 x 10^{-14} s. Also shown in Figure 5b is a fit to the temperatures at which a peak was observed in $\tan\delta$, as measured by dielectric spectroscopy at frequencies of 0.001-1.37 kHz [54]: $\ln\omega$ = 19.3 (± 1.0) – 2954 (± 220)/T_m.

The rounded peak in Q^{-1} at ~75 K is well defined in the accumulated data shown in Figure 5a, but an additional peak in the vicinity of 130 K was observed for only a small number of resonances and did not appear to have a systematic dependence on frequency.

4.2 ErMnO$_3$ Crystal 1 in magnetic field, H//c

4.2.1 Variable temperature at constant field

Figure 6 shows variations of f^2 and Q^{-1} from a resonance peak with frequency near 1170 kHz in spectra from the 12.4 mg piece of Crystal 1, for cooling/heating cycles through the interval 2-100 K at fixed field strengths of 0.06, 0.25, 0.5, 0.75, 1 T (H//c). The field was set when the crystal was at 100 K before each cooling/heating cycle and increased to the next fixed value at the start of the next cycle. The sequence ended because the crystal fell out of the sample holder when the temperature was reduced

to 6 K with the field set at 1 T. Overall, variations of f^2 and Q^{-1} were much the same as in zero field: slight elastic softening as T_N was approached from above with a sharp break in slope of f^2 at ~80 K and stiffening by ~1.2%. The peak in Q^{-1} at ~75 K appears to be unchanged between different field strengths.

Small differences in the evolution of f^2 at the lowest temperatures are shown more clearly in Figure 7a (cooling), which contains data from a resonance peak with frequency near 580 kHz from the same spectra as the peak shown in Figure 6. Figure 7b shows the variations during heating. Slight but distinct softening with falling temperature between 5 and 3 K is evident in the data collected at 0.06 and 0.25 T (see inserts in Fig. 6a,b). Softening by up to ~0.5% occurred below ~15 K during cooling in a field of 0.5 T (Fig. 6c, 7a). This softening was retained, irreversibly, on reheating and in subsequent cooling/heating cycles at 0.75 and 1 T. Essentially the same pattern of reversible and irreversible changes was observed for all the other resonance peaks in the primary spectra.
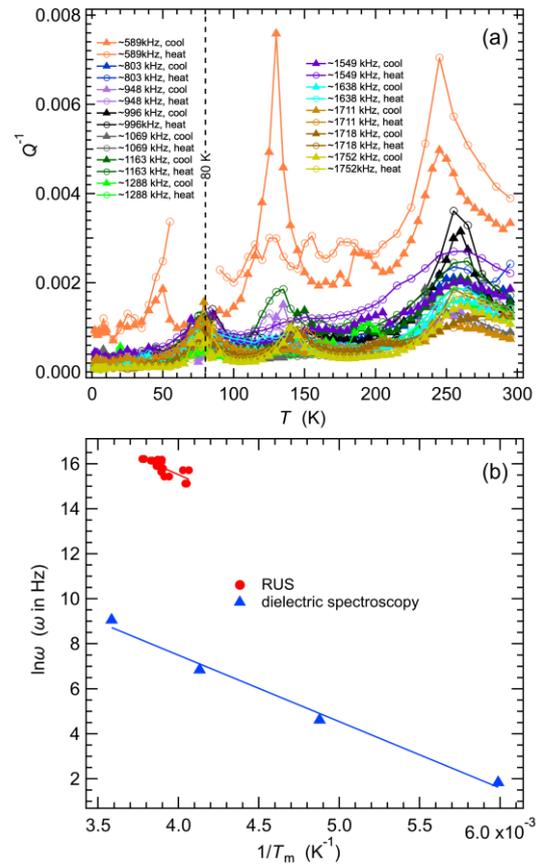
Fig. 5. (a) Q^{-1} variations from resonance peaks with the approximate frequencies listed in the captions, from spectra collected using the 12.4 mg piece of Crystal 1 with its long axis aligned parallel to the faces of the transducers. (b) Arrhenius plots of RUS data from fitting of the peaks near 250 K with Equation 1 and of dielectric spectroscopy data for the temperatures at which a peak in $\tan\delta$ was observed by Ruff et al. [56].

The RUS data for zero field in Figure 3 show a small drop in f^2 values between 3 and 2 K, indicating that the AFM to FIM$_1$ transition is accompanied by a small degree of softening. On the basis of Figure 1, the transition at 0.06 and 0.25 T should be AFM to FIM$_2$. The amount of softening below ~5 K at these field strengths was slightly greater than for AFM → FIM$_1$ (Fig. 6a,b,7), which means that the effect of changing from multidomain to single domain is to induce an additional small degree of elastic softening of the crystal as a whole. Heat capacity data from the literature show anomalies below 5 K which confirm unambiguously that the change from AFM to FIM$_1$/FIM$_2$ is due to a discrete phase transition [7,45].

By way of contrast with the elastic anomalies below 5 K, the larger, relatively steep and irreversible softening which developed during cooling below ~15 K at 0.5 T (Fig. 6c) does not correlate with any of the boundaries between stability fields. Furthermore, measurements of heat capacity in magnetic fields of between 0 and 2 T do not show any anomalies which might signal a phase transition between 10 and 30 K [45]. It is likely, therefore, that the elastic anomaly below 15 K at 0.5 T arose as a consequence of some change in microstructure. Given that the extra softening was maintained at 0.75 and 1 T during heating even to temperatures above the Néel point (Fig. 7), this must have included a change in the configuration of ferroelectric domains. As discussed below, variations in bulk elastic properties of the crystal would include contributions of piezomagnetic and piezoelectric coefficients when the proportions of differently oriented domains changed.
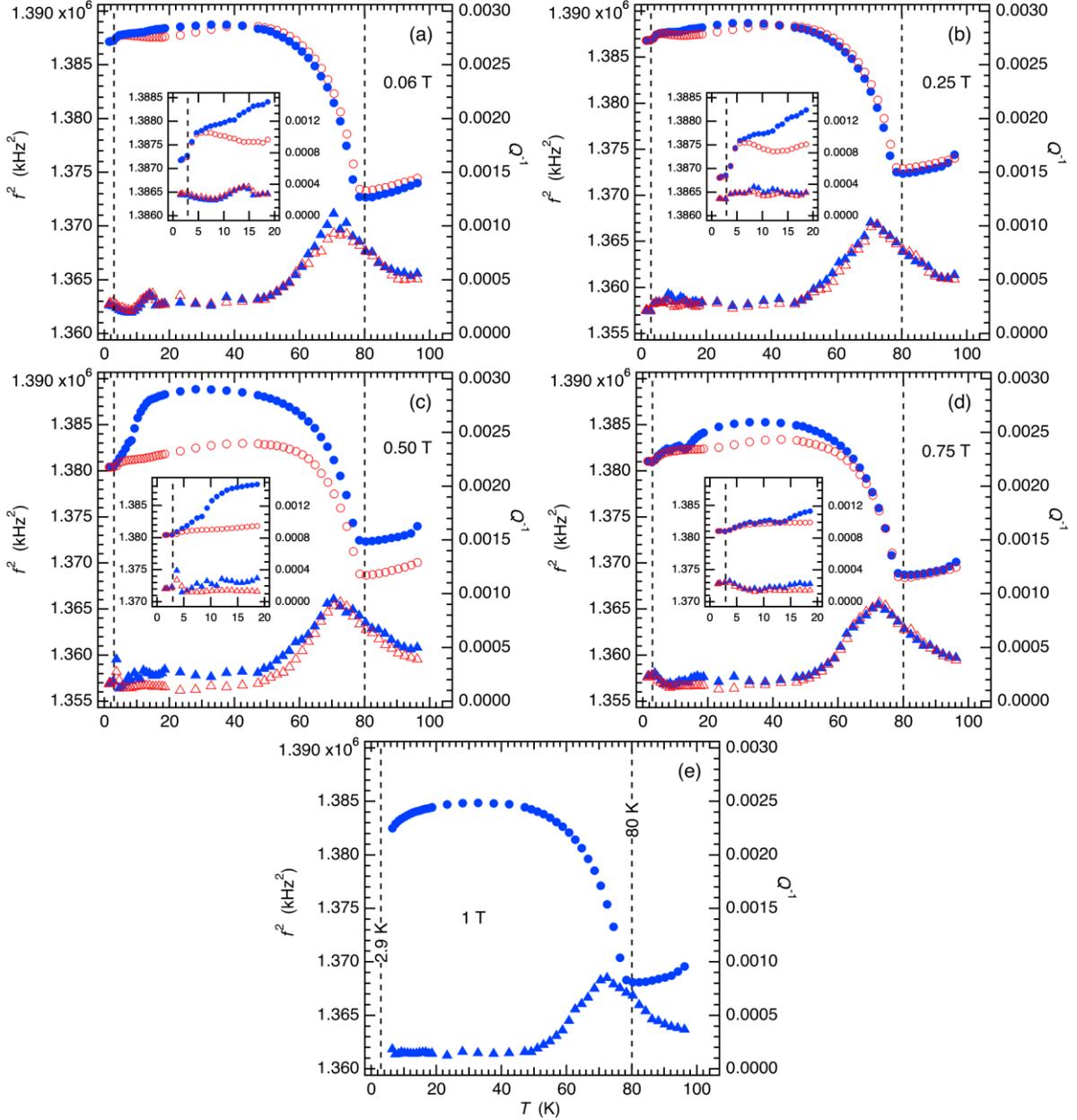
Fig. 6. Details of f^2 and Q^{-1} variations for a resonance peak with frequency near 1170 kHz in spectra collected during cooling, followed by heating, between 100 and 2 K in an applied magnetic field ($H//c$). Blue filled symbols = cooling, open red symbols = heating. 12.4 mg piece of Crystal 1. The field was increased to a new (higher) value when the temperature was at 100 K at the start of each cycle. Apparent peaks in the data for Q^{-1} at temperatures below ~25 K were not reproducible between runs and are considered to be artefacts. The vertical broken line at 80 K marks the expected Néel point and the broken line at 2.9 K marks the temperature for the AFM – FIM_1 transition estimated from Figure 3. Inserts show data in the temperature range 5-20 K at higher magnification.

4.2.2 Variable field at constant temperature

The first attempt to collect spectra as a function of increasing field at 1.6 K ended with the 20 mg crystal being displaced from the sample holder when the field was increased from 1 to 1.2 T. Reversing the field reverses the direction of the force on the crystal due to interaction with the induced moment, so it was warmed to room temperature, remounted and cooled back to 1.6 K. With the direction of field reversed, spectra were collected successfully to –2.4 T before the crystal again fell out of the sample holder. Results from selected resonances are displayed in Figure 8. The spectra were unusually noisy at low fields for reasons that could have been purely experimental, so only the most robust data for Q^{-1} between ~0 and –0.2 T are shown. They display a small peak at ~-0.05 T. . Resonances with frequencies near 630, 880, 1070, and 1180 kHz at first softened and then stiffened slightly without any obvious further features. The

resonances with frequencies near 610 and 700 kHz stiffened more steeply and show two step-like changes in f^2 values at ~-0.275 and ~-0.425 T. These two groups of peaks must be representative of the evolution of two different combinations of elastic moduli. No evidence of a metamagnetic transition was seen throughout the full range to –2.4 T.

The 20 mg crystal broke into two pieces when it was displaced from the sample holder at –2.4 T. The 12.4 mg fragment was remounted for measurements under variable field at 2 K but became displaced from the sample holder at –0.46 T (H//c). After reheating to room temperature, remounting and cooling back to 2 K, it proved possible to collect spectra while cycling the magnetic field between +0.44 and –0.44 T. The results for f^2 and Q^{-1} from a resonance peak with frequency near 550 kHz are shown in Figure 9a. Starting from zero field, f^2 remained approximately constant until ~–0.08 T, softened to a minimum at ~–0.15 T, increased to a maximum at ~–0.35 T and finally decreased back to a low value at –0.44 T. The full range of f^2 values implies a total variation of the corresponding shear elastic moduli by up to ~0.6%. Two cycles between +0.44 T and –0.44 T then gave symmetrical concave-down curves such that f^2 values at +0.44 and -0.44 T were essentially the same and show variations by up to 0.2%. The primary spectra were less noisy than those collected at low fields in the earlier run up to –2.4 T and yielded more or less constant values of Q^{-1}, consistent with the view that the loss peak evident between 0 and –0.2 T in Figure 8 is most likely to have been an artefact.

Fig. 8. f^2 (filled circles) and Q^{-1} (open circles) variations as a function of magnetic field (H//c) for selected resonance peaks in spectra collected with increasing field at 1.6 K (Crystal 1, 20 mg). f^2 values for each resonance peak have been scaled arbitrarily along the y-axis in order to allow easy comparison of how they evolve. The spectra were particularly noisy at low fields, with the result that the peak in Q^{-1} at ~–0.1 T may or may not be real.

Magnetic hysteresis loops reported in the literature (Fig. 2a of ref. [20], Fig. 4a of ref. [16]) show that ErMnO$_3$ displays a pattern of ferrimagnetic opening between ~+0.5 and ~–0.5 T at ~2 K. For comparison with the f^2 results in Figure 9a, data from Fiebig et al. [20] are reproduced in Figure 9b, in which Faraday rotation angle on the y-axis is a proxy for net moment. In both figures, the initial response to increasing field differs from the pattern of cycling which follows. The most straightforward explanation of the observed pattern of elastic softening and stiffening is that it is due to changes in net piezomagnetic properties of the bulk crystal associated with poling of the ferrimagnetic domains. The starting state would have been a crystal with zero net moment, i.e. with equal proportions of ferrimagnetic domains with moments parallel and anti-parallel to the c-axis. Path 1 in Figure 9a is then a reflection of how the contributions of individual ferrimagnetic domains to the bulk elastic/piezomagnetic properties evolved as they rotated or reversed towards the poled state at ~–0.4 T. Once poled, reversing the field induced a reversal of moments through a different pathway of domain states with different bulk properties. A repetitive sequence of domain states and elastic properties then occurred in subsequent cycles. On this basis, the combined contributions of elastic and piezomagnetic moduli, as represented by values of f^2, should be the same for plus and minus directions of moments in the poled crystal, as is observed. These changes in domain configurations were not associated with any obvious variations in acoustic loss.

Fig.7. f^2 and Q^{-1} variations for a resonance peak with frequency near 580 kHz in the same spectra as used to extract results for the 1170 kHz peak in Figure 6a-e. The vertical broken line at 80 K marks the expected Néel temperature. An irreversible reduction in f^2 values occurred below ~15 K during cooling in a field of 0.5 T and the crystal became displaced from the sample holder below 6 K during cooling in a field of 1 T.

Fig. 9. (a) Hysteresis sequence at 2 K for f^2 (filled circles) and Q^{-1} (open circles) from a resonance peak with frequency near 550 kHz: $0 \rightarrow -0.44$ T (first cycle), -0.44 T $\rightarrow +0.44$ T (second cycle), $+0.44 \rightarrow -0.44$ T (third cycle), in 0.02 T steps ($H//c$). (b) Magnetic hysteresis loop reproduced from Fiebig et al. [20] from a different crystal, also at 2 K and $H//c$. Faraday angle scales with magnetic moment. The full sequence was between $+1.5$ and -1.5 T, but only the segments between $+0.6$ and -0.6 T are shown.

There must also be a classical magnetoelastic contribution from changes in elastic moduli due to field-induced lattice distortions associated with increasing net moment of the crystal, but the evidence from higher fields (Fig. 8) is that this results in elastic stiffening rather than softening.

4.3 ErMnO₃ Crystal 2

Crystal 2 was held in the RUS sample holder with its long direction parallel to the faces of the transducers. Its crystallographic orientation was not known, but this more stable configuration allowed a higher magnetic field to be applied before it became displaced. f^2 and Q^{-1} data from selected peaks in RUS spectra collected between 5 and 295 K are shown in Figure 10. All the resonance peaks showed the same initial stiffening (increasing values of f^2) with falling temperature as seen for Crystal 1. An interval of slight softening occurred as $T \rightarrow T_N$ followed by stiffening by up to ~2% at $T < T_N$. The peak in Q^{-1} at ~75 K was weaker than seen in the data from Crystal 1 but is still identifiable (Fig. 10b). The evolution of f^2 for all resonances over the full temperature range was more nearly reversible between cooling and heating than seen for Crystal 1, but thermal treatments were not identical. Crystal 1 was cooled to below the AFM – FIM₁ transition while Crystal 2 was only cooled to 5 K.
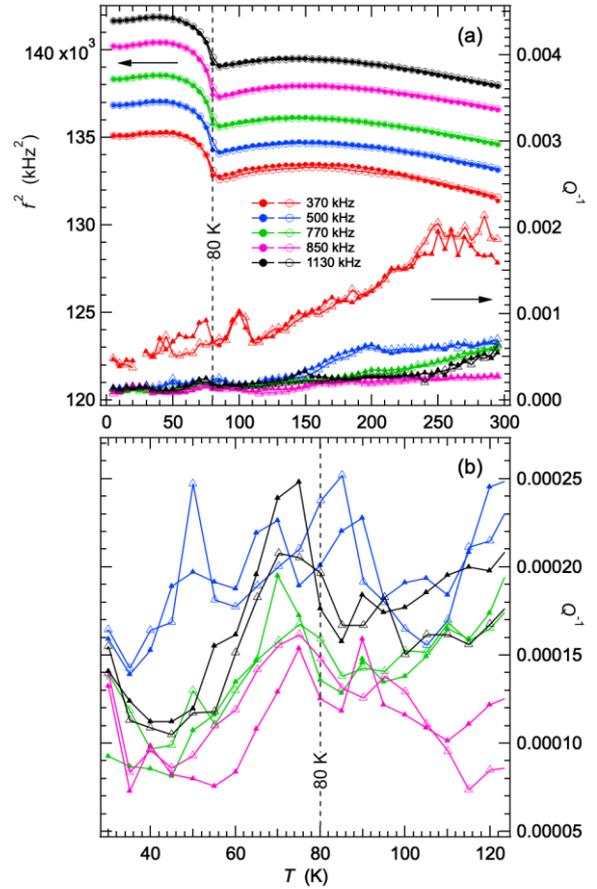
Fig. 10. Crystal 2. (a) f^2 (circles) and Q^{-1} (triangles) variations as a function of temperature for several resonance peaks in spectra collected in 5 K steps through the temperature interval 5–295 K. Open symbols = heating, filled symbols = cooling. f^2 values for each resonance peak have been scaled arbitrarily along the y-axis in order to allow easy comparison of how they each evolved. (b) Expansion of Q^{-1} data to show that there may still be a weak peak ~5 K below T_N.

Of particular interest was the form of elastic anomaly that would be observed at the AFM $\rightarrow$ FM transition driven by increasing field. Figure 11 shows a stack of segments of spectra and values of f^2 and Q^{-1} obtained as a function of increasing magnetic field strength at 5 K. The crystal became displaced from the sample holder on increasing the field above 10.4 T, demonstrating that some net moment had indeed been induced. All the resonances indicate a very slight softening in the initial field up to ~0.5 T followed by elastic stiffening with increasing field and a number of discontinuities (Fig. 11b). The AFM $\rightarrow$ FM transition is expected to occur at ~2–3 T when the field is applied parallel to [001] but does not occur when the field direction is within the (001) plane [7,22,44]. The discontinuity between 4 and 4.2 T is the largest of the changes in f^2 and indicates abrupt stiffening of all the elastic moduli. It is accompanied by changes in Q^{-1} (increasing loss on the high field side) and is therefore most likely to have marked a phase transition. The smaller discontinuities involve both softening and stiffening, are not accompanied by changes in loss, and would then represent jerky/abrupt changes in the configuration of magnetic and/or ferroelectric domain walls.
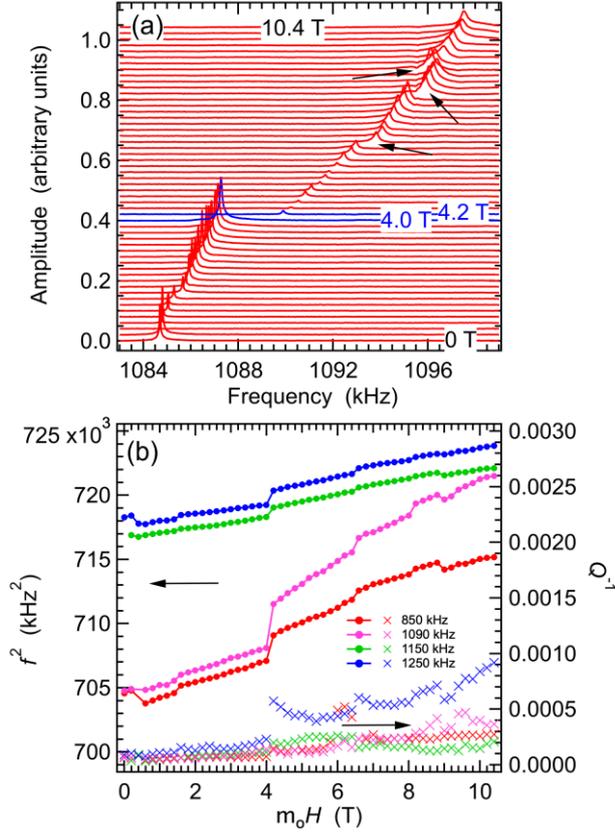
Fig. 11. (a) Stack of segments of RUS spectra showing the effect of increasing magnetic field at 5 K on a resonance peak near 1090 kHz from ErMnO$_3$ Crystal 2. The spectra have been offset up the y-axis in proportion to the strength of the applied field. There is a break in the trend of peak frequency with temperature near 0.5 T and a very obvious discontinuity between 4.0 and 4.2 T. Arrows point to jogs in the evolution of individual resonance peaks at ~6.5, ~8.1 and ~8.9 T. The crystal was displaced from the sample holder when the field was increased from 10.4 to 10.6 T. (b) f^2 (filled circles) and Q^{-1} (crosses) variations as a function of the magnetic field at 5 K for several resonance peaks, including the one shown in (a) which had frequency near 1090 kHz. Values of f^2 have been scaled arbitrarily along the y-axis to allow the trends shown by each resonance to be compared.

4.4 Er$_{0.99}$Zr$_{0.01}$MnO$_3$§

Variations of f^2 and Q^{-1} from resonance peaks in spectra collected during cooling and heating in 5 K steps between 5 and 295 K for the Zr-doped crystal, Er$_{0.99}$Zr$_{0.01}$MnO$_3$, are shown in Figure 12. The shape and mass of the crystal was different from the two ErMnO$_3$ crystals, so the combination of elastic moduli represented by the individual resonances would again have been different. The overall pattern has essentially the same form as for the second crystal of pure ErMnO$_3$ (Fig. 10a). Stiffening by up to ~2% occurred below T_N, but there is no obvious peak in Q^{-1} at ~75 K. Differences in the values of f^2 between heating and cooling in the temperature interval ~30-240 K are larger than seen for Crystal 2. As for both the pure crystals, Q^{-1} for at least some of the resonances has a rounded maximum in the vicinity of 270 K.
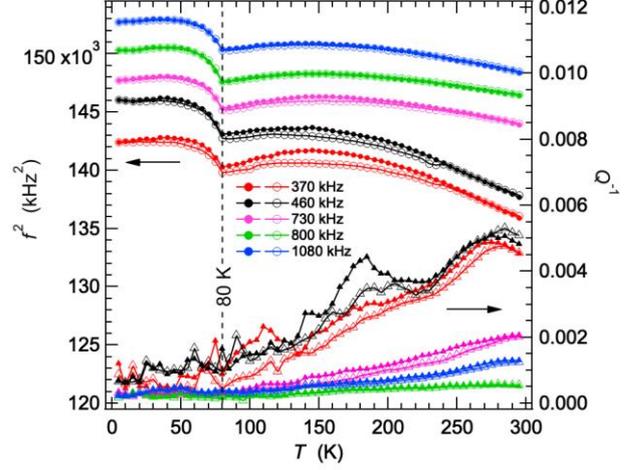
Fig. 12. f^2 and Q^{-1} variations as a function of temperature collected during cooling (filled symbols) and heating (open symbols) for several resonance peaks in spectra from a single crystal of Er$_{0.99}$Zr$_{0.01}$MnO$_3$ in the temperature interval 5-295 K. f^2 values for each resonance peak have been scaled arbitrarily along the y-axis in order to allow easy comparison of how they evolve.

5. Discussion

5.1 Strain/order parameter coupling

The overall pattern of changes in elastic properties associated with AFM ordering in all three of the crystals considered here is broadly similar to that seen previously for YMnO$_3$ [53]. There is stiffening from room temperature down to ~150 K, below which all resonances of ErMnO$_3$ and some of YMnO$_3$ show slight softening as the temperature approaches T_N (~73 K in YMnO$_3$, ~80 K in ErMnO$_3$). The manner in which f^2 of most resonances increases below 80 K very obviously correlates with the form of observed increases in intensity of magnetic superlattice reflections in neutron diffraction patterns reported by Meier et al. [44] and Park et al. [57] which, in turn, scale with m^2. This is the pattern expected from coupling of the form $\lambda e^2 m^2$, rather than the softening expected from coupling of the form $\lambda e m^2$, and is consistent with the view that the relaxation time for the response of the magnetic order parameter to changes in strain is longer than ~10^{-6} s. The obvious contrast for YMnO$_3$ and ErMnO$_3$ is with AFM ordering in CoF$_2$ where a classical pattern of softening below T_N implies faster relaxation of the order parameter in response to an induced strain [54].

Differences between YMnO$_3$ and ErMnO$_3$ reveal the more subtle influence of ordering of moments of Er^{3+}, since Y^{3+} does not have a magnetic moment. The crystallographic space group of YMnO$_3$ and ErMnO$_3$ at room temperature and below is $P6_3cm$. They have more or less the same Néel temperature but different magnetic ordering schemes. The magnetic space group reported for YMnO$_3$ below T_N is $P6_3'cm'$ [58], while that for ErMnO$_3$ is $P6_3'c'm$, changing to $P6_3c'm'$ at low temperature [44]. The magnetic structure of ErMnO$_3$ includes the influence of moments at Er on 4b sites which order, triggered by the moments at Mn [44]. The fact that the evolution of elastic stiffening below T_N is at the level of up to ~2% and essentially the same in both YMnO$_3$ and ErMnO$_3$, together with the observation that any further changes at the lowest temperatures in ErMnO$_3$ are at a level of only 0.03% (Fig. 3), shows that coupling of strain with ordering of magnetic moments of Er^{3+} is very much weaker than coupling of strain with the order parameter for magnetic moments at Mn^{3+}.

Another subtle but revealing difference between YMnO$_3$ and ErMnO$_3$ is that there is a peak in Q^{-1} associated with the PM – AFM transition in ErMnO$_3$ (Fig. 2,4,5) but not in RUS data from YMnO$_3$ [53]. If it was due to critical slowing down of some

component of the structure at the transition point, it would be expected to show a sharp maximum at the Néel point, as seen in CoF_2 [54]. Instead, the peak is rounded, has its maximum ~5 K below T_N and more nearly resembles a typical Debye-like loss peak with $E_a \geq$ ~0.05 eV. A peak seen in Q^{-1} data from orthorhombic $GdMnO_3$ at ~80 K yielded a similar activation energy, $\geq$ ~0.04 eV, and was attributed to freezing of polaron-like strain clouds around local dynamical magnetic/electric dipoles [42]. The most obvious loss mechanism in $ErMnO_3$ involves freezing of moments of Er^{3+} at 4b sites, driven by favourable coupling of strain fields arising from these moments with strain fields due to the long range ordering of moments at Mn^{3+} sites.

The onset of irreversible changes in f^2 values on cooling below ~15 K at 0.5 T does not coincide with any discrete phase boundary in Figure 1, and is interpreted here as being related to an onset of ordering of moments at Er on 2a sites, which Figure 6c of Meier et al. [44] shows as preceding the AFM $\rightarrow$ FIM transition in zero field, and changes in microstructure. Evidence of the onset of some additional but continuous structural or magnetic relaxation ahead of the transition in Crystal 1 is also provided by the break in slope of f^2 variations shown by selected resonances. For example, resonance peaks with frequencies near 1070, 1300, 1715 kHz in Figure 2, and near 690, 880 kHz in Figure 4 show stiffening rather than softening with falling temperature below ~40 K.

By way of contrast with small changes due to poling of the FIM structure, evidence of a metamagnetic transition between 4.0 and 4.2 T at 5 K (Fig. 11) is provided by the sharp and relatively large discontinuity in the frequencies of all the resonance peaks. On the basis of group-subgroup arguments (below), the AFM ($P6_3'c'm$) $\rightarrow$ FM ($P6_3'c'm'$) transition must be first order, but the larger changes in f^2 values imply larger differences between the elastic moduli and/or piezo coefficients of the AFM and FM structures in comparison with between the AFM and FIM structures. This is consistent with the expectation that coupling between the magnetic order parameter and strain should be stronger when all the moments at Er^{3+} are aligned in the same direction (FM) as opposed to when they are ordered antiferromagnetically between 4a and 2b sites (FIM).

5.2 Contribution of piezomagnetic and piezoelectric effects

$P6_3c'm'$ is not a subgroup of $P6_3'c'm$ [56] with the consequence that, if the space groups given in the literature are correct, the AFM – FIM transition at ~2.5 K must be first order. This is consistent, at least, with the abruptness of changes in f^2 (Fig. 2,3). Differences in elastic moduli between the two magnetic structures would contribute directly to the observed changes in f^2 but there may also be contributions from piezomagnetic and piezoelectric coefficients. Both the AFM and FIM structures are piezoelectric (due to being ferroelectric) and piezomagnetic [58]. In an unpoled crystal, i.e. with all possible domain orientations present in equal proportions, the piezoelectric and piezomagnetic coefficients will not contribute to the bulk elastic properties, but their influence will be present in resonance frequencies of a poled crystal. Quantitative determination of piezoelectric coefficients by Resonant Ultrasound Spectroscopy has been illustrated in the case of $La_3Ga_5SiO_{14}$ and $La_3Ga_{5.5}Ta_{0.5}O_{14}$, for example [59], and the possibility of piezomagnetic contributions has already been discussed for the case of $YMnO_3$ [53].

In the absence of any actual data for values of the piezoelectric and piezomagnetic coefficients, it can still be anticipated that the former will be substantially greater than the latter. Individual spontaneous strains arising at the structural/ferroelectric transition in $YMnO_3$ have values up to ~0.008, while the strains arising at the magnetic transition are an order of magnitude smaller [53]. This is an overt consequence of

the fact that the ferroelectric moment occurs as a result of symmetry-breaking atomic displacements while magnetic ordering does not require any movements of the atoms. Lee et al. [60] referred to the PM – AFM transition as having "giant" magneto-elastic coupling because they detected displacements of atoms associated with the AFM ordering, but the changes in elastic moduli due to coupling of the form $\lambda e^2 m^2$ are only up to ~2%.

Small differences in the degree of softening between AFM $\rightarrow$ FIM$_1$ and AFM $\rightarrow$ FIM$_2$ (Fig. 6, 7), together with correlations between the magnetic and elastic hysteresis loops (Fig. 9), are consistent with the view that small changes in f^2 values at low temperatures in $ErMnO_3$ are related to poling of ferrimagnetic domains in a magnetic field and can be understood in terms of the contribution of piezomagnetic effects, as well as possible piezoelectric effects. The latter would arise if ferroelectric domain walls were displaced along with the magnetic ones. Bilinear magneto-electric coupling is allowed under the $P6_3c'm'$ symmetry of the FIM and FM structures and not under space group $P6_3'c'm$ of the AFM structure [58]. It is also well established that ferroelectric and magnetic domain walls interact in hexagonal manganites [35-39]. Local ferrimagnetic moments or an external magnetic field could therefore induce some displacement of ferroelectric domain walls in the FIM and FM structures but not in the AFM structure. The additional changes observed during cooling below ~15 K in a field of 0.5 T (Fig. 7) provide indirect evidence that ferroelectric domain walls were displaced by the magnetic field as the softening persisted during reheating to above 80 K, i.e. into the stability field of the PM structure where the only domain structure would be ferroelectric. Further hysteretic variations attributable to changes in domain configurations occurred in a 0.75 T field (Fig. 6,7) and would presumably have continued also at higher fields. However, the crystal became displaced from the sample holder on cooling below 6 K at 1 T.

5.3 Domain wall pinning/relaxation

The possible role of defects in pinning domain walls has been considered in detail for hexagonal manganites [61,62], while patterns of acoustic loss at kHz/MHz frequencies have provided insights into the dynamics of point defects and microstructures that are coupled with strain, as seen in numerous examples of freezing/pinning of ferroelastic twin walls in perovskites [41]. None of the domain walls in $ErMnO_3$ have a ferroelastic component, however, and they therefore should not be mobile under the influence of an externally applied shear stress.

Although the domain walls of $ErMnO_3$ do not have any ferroelastic component, Wang et al. [43] have shown that shear stress applied to thin (0.02 mm) crystals at temperatures of ~1100 °C can induce movement of vortices and antivortices in opposite directions, leading to changes in the distribution of individual domain walls. Any dynamic motion of vortices induced by shear stresses within acoustic resonances of a mm-sized crystal would give rise to high loss if the relaxation time was ~10^{-6} s, but no evidence for this has been found in the RUS results. The stress/strain conditions that were applied by Wang et al. [43], both in terms of temperature and load, were very different from the shear strains in an acoustic resonance of a small crystal below room temperature. Instead, evidence for ferroelectric and/or magnetic domain wall motion is provided by abrupt changes in some resonance frequencies in Figures 6 and 9 which can be understood in terms of jerky displacements from one pinned position to another under the influence of magnetic field.

In addition to the softening observed during cooling at 0.5 T being maintained to temperatures above T_N, evidence of changes in magnetic and ferroelectric domain wall configurations is

provided by irreversibility seen in the evolution of f^2 values in temperature cycles between 2 and 100 K in zero field (Fig. 4). Hysteresis of f^2 values between cooling and heating starts at ~30 K in the heating sequence and, in the more extensive sequences, the values return to a reversible pattern above ~250 K. A similar pattern of hysteresis was seen between ~30 and ~240 K for Crystal 2 and the crystal of $Er_{0.99}Zr_{0.01}MnO_3$ (Fig. 10,12). The origin of this has not been determined unambiguously but is likely to have been due to small changes in ferroelectric domain configurations arising from magnetoelectric coupling effects at the lowest temperatures. Self-induced changes in microstructure associated with the influence of internal magnetic fields and magnetic domains arise from ordering of moments at Er^{3+}. If a new magnetically driven configuration of local ferroelectric domain wall positions was pinned by defects, it would persist to high temperatures. The temperature dependence of f^2 values returns to a reversible pattern above ~250 K which would then correspond to the temperature above which relaxation of domain walls pinned at lower temperatures can return to their original configuration. Evidence for backswitching has been seen also in $YMnO_3$ where changes in domain configurations induced by an electric field at 120 K returned to their original positions when heated to 250 K [63].

Dynamic coupling between strain and electric dipole effects is implied by the correlation between increasing values of Q^{-1} with increasing temperature up to at least ~300 K for all three crystals reported here and increases in dielectric loss, $\tan\delta$, reported for frequencies of 0.1–1 MHz by Ruff et al. [56]. Closely similar increases of Q^{-1} were also observed in RUS results from hexagonal $YMnO_3$ [53]. However, as shown in Figure 5, the peak in $\tan\delta$ data from the Supplementary Material of Ruff et al. [56] does not correlate quantitatively with the peak in Q^{-1} near 250 K when treated as representing the condition $\omega\tau = 1$. Although the activation energies extracted from the two sets of data overlap, 0.25 ± 0.02 eV from $\tan\delta$ and 0.28 ± 0.06 eV from Q^{-1}, the relaxation time derived from the dielectric loss is orders of magnitude slower at ~10^{-9} s rather than ~10^{-13} s.

Previously reported values of activation energy for the migration of ferroelectric domain walls in $YMnO_3$ and $ErMnO_3$ include 0.24 eV [61] and 0.54 eV [64] respectively. The loss peak in Q^{-1} is therefore also likely to be due to pinning/unpinning of some aspect of the ferroelectric domain structure which remains mobile under the low stress, high frequency conditions of an RUS experiment only above ~250 K. Changes induced in the ferroelectric domain wall configurations or whatever changes of other defects that occur as a consequence of cycling through the AFM – FIM transition relax back to the starting state after the crystals are heated back to temperatures above the (frequency-dependent) freezing/pinning temperature. This correlates with the more direct observations of domain wall pinning below ~250 K in $YMnO_3$ made by Kuerten et al. [63].

A degree of mobility for ferroelectric domain walls at room temperature is also implied by the observation of Han et al. [65] and Roede et al. [62] that the configuration of domains induced at the surface of a crystal of $ErMnO_3$ by application of external electric field relaxed back to the original configuration when the field was removed.

5.4 Local strain heterogeneity due to chemical doping

Suppression of the loss peak at ~75 K is the most overt acoustic effect of doping $ErMnO_3$ with 1% Zr (Fig. 12), since other features of the elastic properties of the AFM and PM phases of the crystal of $Er_{0.99}Zr_{0.01}MnO_3$ are the same as observed for the two crystals with nominally end member compositions. From the effect of replacing Pr with La on a ferroelastic transition in $PrAlO_3$, it has previously been found that local strain fields around individual impurity atoms in perovskites start to overlap at about 1.6% doping, corresponding

to an effective diameter for each strain field of ~16-18 Å [66]. An inevitable consequence of doping hexagonal $ErMnO_3$ with Zr must be the creation of equivalent local strain heterogeneity arising from the difference in radii of Zr^{4+} and Er^{3+}. On this basis, the local heterogeneity appears to have been sufficient to disrupt strain relaxation accompanying freezing of moments at Er^{3+} on 4b sites and/or the freezing process itself. The associated change in oxygen stoichiometry would further contribute to these local effects.

5.5 Engineering of microstructures

The functional property of $ErMnO_3$ that has attracted attention as having greatest potential for use in device applications is the electrical conductivity of domain walls [4,29,31,33,49,67-71]. For some of the aspirations in this context to be achieved, it will be necessary to engineer domain walls into preferred configurations and then constrain the chosen microstructure to remain stable during long term operation of the device. The ferroelectric domain walls of hexagonal $RMnO_3$ manganites are not ferroelastic, so that it is not expected that application of stress would cause them to move. Nevertheless, there are clearly magnetoelastic effects at low temperatures which have some influence on domain wall mobility in $ErMnO_3$. Simply cooling to the lowest temperatures in zero field appears to result in some degree of self-organisation of the domain walls, and the effect is greater if the cooling is carried out with the crystal held in a magnetic field of 0.5 T. Increasing the field at low temperatures appears to cause jerky motion, indicating that the walls jump between successive pinning points rather than smoothly through the crystal. Further exploration of protocols involving variable field and temperature conditions has the potential to allow manipulation of the microstructures of both bulk and thin film samples which may persist at temperatures below a domain wall pinning/freezing temperature of ~250 K. **6. Conclusions**

The largest magnetoelastic effect observed in multiferroic hexagonal manganites by RUS is stiffening by up to ~2% due to biquadratic coupling of strain with the order parameter for ordering of Mn^{3+} moments. Coupling of strains with Er moments in $ErMnO_3$ is substantially weaker, as seen in smaller changes of bulk elastic properties below ~3 K and subtle changes of elastic properties associated with magnetic poling.

A Debye-like peak in acoustic loss occurs immediately below the PM – AFM transition point in $ErMnO_3$ but not in $YMnO_3$, and is attributed to dynamical strain effects associated with freezing of magnetic moments at Er on 4b sites. Absence of this peak in data from $Er_{0.99}Zr_{0.01}MnO_3$ can be understood in terms of disruption of strain-mediated correlations between moments due to the influence of local strain heterogeneity arising from differences in radii of Zr and Er, with additional contributions potentially from associated changes in oxygen stoichiometry.

Even though domain walls in $ErMnO_3$ are not ferroelastic, variations in the configuration of ferroelectric domains in response both to application of an external magnetic field and to the internal magnetic field of the FIM structure can be detected through the contributions of piezomagnetic and piezoelectric moduli. Jerkiness of changes in response to higher fields implies that domain walls jump from one set of locally pinned positions to another.

A peak in acoustic loss at ~250 K coincides with the upper limit of hysteretic variations of acoustic resonance frequencies between cooling and heating, and has been attributed to pinning/freezing of ferroelectric domain walls by a strain coupling mechanism with an activation energy of ~0.25-0.3 eV.

The overall sensitivity of $ErMnO_3$ to thermal and magnetic history, together with the sensitivity of the RUS method, provide an effective methodology for following and manipulating

multiferroic properties that depend on the configuration of magnetic and ferroelectric domains that are not also ferroelastic.

Declaration of Competing Interest

The authors declare that they have no known competing financial interests or personal relationships that could have appeared to influence the work reported in this paper.

Acknowledgements

ORCID iDs

C.M. Fernandez-Posada: 0000-0003-3080-1637

C.R.S. Haines: 0000-0002-1274-8329

D.M. Evans: 0000-0002-8546-0676

Z. Yan: 0000-0002-9073-6358

E. Bourret: 0000-0002-8487-0112

D. Meier: 0000-0002-8623-6705

M.A. Carpenter: 0000-0003-2855-0007

References

[1] S.C. Abrahams, Acta Cryst. B 57 (2001) 485.
[2] Th. Lonkai, D.G. Tomuta, U. Amann, J. Ihringer, R.W.A. Hendrikx, D.M. Többens, J.A. Mydosh, Phys. Rev. B 69 (2004) 134108.
[3] A.S. Gibbs, K.S. Knight, P. Lightfoot, Phys. Rev. B 83 (2011) 094111.
[4] N.E. Massa, L. del Campo, K. Holldack, A. Canizarès, V. Ta Phuoc, P. Kayser, J.A. Alonso, Phys. Rev. B 102 (2020) 134305.
[5] B.B. Van Aken, T.T.M. Palstra, A. Filippetti, N.A. Spaldin, Nature Materials 3 (2004) 164.
[6] J.-S. Zhou, J.B. Goodenough, J.M. Gallardo-Amores, E. Morán, M.A. Alario-Franco, R. Caudillo, Phys. Rev. B 74 (2006) 014422.
[7] F. Yen, C. dela Cruz, B. Lorenz, E. Galstyan, Y. Sun, M. Gospodinov, C.W. Chu, J. Mat. Res. 22 (2007) 2163.
[8] C. Wehrenfennig, D. Meier, Th. Lottermoser, Th. Lonkai, J.-U. Hoffmann, N. Aliouane, D.N. Argyriou, M. Fiebig, Phys. Rev. B 82 (2010) 100414.
[9] B. Lorenz, Phys. Sci. Rev. 4 (2019) 0014.
[10] M. Fiebig, D. Fröhlich, K. Kohn, St. Leute, Th. Lottermoser, V. V. Pavlov, and R. V. Pisarev, Phys. Rev. Lett. 84 (2000) 5620.
[11] K. Łukaszewicz, J. Karut-Kalicińska, Ferroelectrics 7 (1974) 81.
[12] B.B. Van Aken, A. Meetsma, and T.T.M. Palstra, Acta Cryst. E 57 (2001) i38.
[13] O. Fedorova, G. Kozhina, S. Uporov, J. Alloys Cpds. 740 (2018) 677.
[14] C.J. Fennie, K.M. Rabe, Phys. Rev. B 72 (2005) 100103.
[15] M. Lilienblum, Th. Lottermoser, S. Manz, S.M. Selbach, A. Cano, M. Fiebig, Nature Physics 11 (2015) 1070.
[16] H. Sugie, N. Iwata, K. Kohn, J. Phys. Soc. Jpn 71 (2002) 1558.
[17] E.C. Standard, T. Stanislavchuk, A.A. Sirenko, N. Lee, S.-W. Cheong, Phys. Rev. B 85 (2012) 144422.
[18] N. Iwata, K. Kohn, Ferroelectrics 219 (1998) 161.
[19] M. Fiebig, T. Lottermoser, R.V. Pisarev, J. Appl. Phys. 93 (2013) 8194.
[20] M. Fiebig, C. Degenhardt, R.V. Pisarev, Phys. Rev. Lett. 88 (2001) 027203.
[21] D. Meier, H. Ryll, K. Kiefer, B. Klemke, J.U. Hoffmann, R. Ramesh, M. Fiebig, Phys. Rev. B 86 (2012) 184415.
[22] Y.J. Liu, J.F. Wang, X.F. Sun, J.-S. Zhou, Z.C. Xia, Z.W. Ouyang, M. Yang, C.B. Liu, R. Chen, J.-G. Cheng, Y. Kohama, M. Tokunaga, K. Kindo, Phys. Rev. B 97 (2018) 214419.
[23] S.C. Chae, Y. Horibe, D.Y. Jeong, S. Rodan, N. Lee, S.-W. Cheong, PNAS 107 (2010) 21366).

[24] Yu. Kumagai, N.A. Spaldin, Nature Comm. 4 (2012) 1540.
[25] J. Li, F.-K. Chiang, Z. Chen, C. Ma, M.-W. Chu, C.-H. Chen, H. Tian, H. Yang, J. Li, Scientific Reports 6 (2016) 28047.
[26] M.E. Holtz, K. Shapovalov, J.A. Mundy, C.S. Chang, Z. Yan, E. Bourret, D.A. Muller, D. Meier, A. Cano, Nano Lett. 17 (2017) 5883.
[27] T. Choi, Y. Horibe, H.T. Yi, Y.J. Choi, Weida Wu, S.-W. Cheong, Nature Mat. 9 (2010) 253.
[28] T. Jungk, Á. Hoffmann, M. Fiebig, E. Soergel, Appl. Phys. Lett. 97 (2010) 012904.
[29] D.M.Evans, V. Garcia, D. Meier, M. Bibes, Phys. Sci. Rev. 5 (2020) 20190067.
[30] D. Meier, J. Seidel, A. Cano, K. Delaney, Y. Kumagai, M. Mostovoy, N.A. Spaldin, R. Ramesh, M. Fiebig, Nature Materials 11 (2012) 284.
[31] P.W. Turner, J.P.V. McConville, S.J. McCartan, M.H. Campbell, J. Schaab, R.G.P. McQuaid, A. Kumar, J.M. Gregg, Nano Lett. 18 (2018) 6381.
[32] A.B. Mosberg, E.D. Roede, D. M. Evans, T.S. Holstad, E. Bourret, Z. Yan, A.T.J. van Helvoort, D. Meier, Appl. Phys. Lett. 115 (2019) 122901.
[33] J. Schultheiß, J. Schaab, D.R. Småbråten, S.H. Skjærvø, E. Bourret, Z. Yan, S.M. Selbach, D. Meier, Appl. Phys. Lett. 116 (2020) 262903.
[34] Weida Wu, Y. Horibe, N. Lee, S.-W. Cheong, J.R. Guest, Phys. Rev. Lett. 108 (2012) 077203.
[35] M. Fiebig, Th. Lottermoser, D. Fröhlich, A.V. Goltsev, R.V. Pisarev, Nature 419 (2002) 818.
[36] M. Fiebig, Th. Lottermoser, Th. Lonkai, A.V. Goltsev, R.V. Pisarev, J. Magn. Magn. Mat. 290-291 (2005) 883.
[37] Y. Geng, N. Lee, Y.J. Choi, S.-W. Cheong, W. Wu, Nano Lett. 12 (2012) 6055.
[38] Y. Geng, H. Das, A.L. Wysocki, X. Wang, S.-W. Cheong, M. Mostovoy, C.J. Fennie, W. Wu, Nature Materials 13 (2013) 163.
[39] J. Schaab, M. Trassin, A. Scholl, A. Doran, Z. Yan, E. Bourret, R. Ramesh, and D. Meier, J. Phys.: Conf. Ser. 592 (2015) 012120.
[40] M. Giraldo, Q.N. Meier, A. Bortis, D. Nowak, N.A. Spaldin, M. Fiebig, M.C. Weber, T. Lottermoser, Nature Comm. 12 (2021) 3093.
[41] M.A. Carpenter, J. Phys. Cond. Matt. 27 (2015) 263201.
[42] M.A. Carpenter, D. Pesquera, D. O'Flynn, G. Balakrishnan, N. Mufti, A.A. Nugroho, T.T.M. Palstra, M. Mihalik jr, M. Mihalik, M. Zentková, A. Almeida, J. Agostinho Moreira, R. Vilarinho, D Meier, J. Phys.: Cond. Matt. (2020) in press
[43] X. Wang, M. Mostovoy, M.G. Han, Y. Horibe, T. Aoki, Y. Zhu, and S.-W. Cheong, Phys. Rev. Lett. 112 (2014) 247601.
[44] D. Meier, H. Ryll, K. Kiefer, B. Klemke, J.-U. Hoffmann, R. Ramesh, M. Fiebig, Phys. Rev. B 86 (2012) 184415.
[45] J.D. Song, C. Fan, Z.Y. Zhao, F.B. Zhang, J.Y. Zhao, X.G. Liu, X. Zhao, Y.J. Liu, J.F. Wang, X.F. Sun, Phys. Rev. B 96 (2017) 174425.
[46] J.R. Sahu, A. Ghosh, A. Sundaresan, C.N.R. Rao, Mater. Res. Bull. 44 (2009) 2123.
[47] M.C. Lin, Y.S. Chen, T.C. Han, J.G. Lin, C.H. Chen, Ferroelectrics 380 (2009) 38.
[48] T. Kyômen, M. Morita, M. Itoh, K. Kohn, N. Kamegashira, Ferroelectrics 264 (2001) 223.
[49] T.S. Holstad, T.R. Ræder, D.M. Evans, D.R. Småbråten, S. Krohns, J. Schaab, Z. Yan, E. Bourret, A.T.J. van Helvoort, T. Grande, S.M. Selbach, J.C. Agar, D. Meier, npj Comp. Mat. 6 (2020) 163.
[50] A. Migliori, J.L. Sarrao, Resonant Ultrasound Spectroscopy: Applications to Physics, Materials Measurements and Nondestructive Evaluation, Wiley, New York, 1997.
[51] J. Schiemer, L.J. Spalek, S.S. Saxena, C. Panagopoulos, T. Katsufuji, A. Bussmann-Holder, J. Köhler, M.A. Carpenter, Phys. Rev. B 93 (2016) 054108.
[52] D.M. Evans, J.A. Schiemer, M. Schmidt, H. Wilhelm, M.A. Carpenter, Phys. Rev. B 95 (2017) 094426.
[53] R.I. Thomson, T. Chatterji, C.J. Howard, T.T.M. Palstra, M.A. Carpenter, J. Phys.: Cond. Matt 26 (2014) 045901.
[54] R.I. Thomson, T. Chatterji, M.A. Carpenter, J. Phys. Cond. Matt. 26 (2014) 146001.
[55] M. Weller, G.Y. Li, J.X. Zhang, T.S. Kê, J. Diehl, Acta Met. 29 (1981)1047.
[56] A. Ruff, Z. Li, A. Loidl, J. Schaab, M. Fiebig, A. Cano, Z. Yan, E. Bourret, J. Glaum, D. Meier, S. Krohns, Appl. Phys. Lett. 112 (2018) 182908.
[57] J. Park, U. Kong, S.I. Choi, J.-G. Park, C. Lee, W. Jo, Appl. Phys. A 74 (2002) s802.
[58] C.J. Howard, B.J. Campbell, H.T. Stokes, M.A. Carpenter, R.I. Thomson, Acta Cryst. B 69 (2013) 534.
[59] J. Schreuer, IEEE Trans. Ultrasonics, Ferroelectrics, Freq. Cont. 49 (2002) 1474.
[60] S. Lee, A. Pirogov, M. Kang, K.-H. Jang, M. Yonemura, T. Kamiyama, S.-W. Cheong, F. Gozzo, N. Shin, H. Kimura, Y. Noda, J.-G. Park, Nature Lett. 451 (2008) 805.
[619] D.R. Småbråten, T.S. Holstad, D.M. Evans, Z. Yan, E. Bourret, D. Meier, S.M. Selbach, Phys. Rev. Res. 2 (2020) 033159.

[62] E.D. Roede, A.B. Mosberg, D.M. Evans, E. Bourret, Z. Yan, A.T.J. van Helvoort, D. Meier, arXiv:2012.00418v1.

[63] L. Kuerten, S. Krohns, P. Schoenherr, K. Holeczek, E. Pomjakushina, T. Lottermoser, M. Trassin, D. Meier, M. Fiebig, Phys. Rev. B 102 (2020) 094108.

[64] A. Barbour, A. Alatas, Y. Liu, C. Zhu, B.M. Leu, X. Zhang, A. Sandy, M.S. Pierce, X. Wang, S.-W., Cheong, H. You, Phys. Rev. B 93 (2016) 054113.

[65] M.-G. Han, Y. Zhu, L. Wu, T. Aoki, V. Volkov. X. Wang, S.C. Chae, Y.S. Oh, S.-W. Cheong, Adv. Mater. 25 (2013) 2415.

[66] C.J. Howard, Z. Zhang, M.A. Carpenter, K.S. Knight, Phys. Rev. B 76 (2007) 054108.

[67] J. Schaab, S.H. Skjærvø, S. Krohns, X. Dai, M.E. Holtz, A. Cano, M. Lilienblum, Z. Yan, E. Bourret, D.A. Muller, M. Fiebig, S.M. Selbach, D. Meier, Nature Nanotech. 13 (2018) 1028.

[68] T.S. Holstad, D.M. Evans, A. Ruff, D.R. Småbråten, J. Schaab, Ch. Tzschaschel, Z. Yan, E. Bourret, S.M. Selbach, S. Krohns, D. Meier, Phys. Rev. B 97 (2018) 085143.

[69] H. Schmidt, Appl. Phys. Lett. 118 (2021) 140502.

[70] L. Puntigam, J. Schultheiß, A. Strinic, Z. Yan, E. Bourret, M. Altthaler, I. Kézsmárki, D.M. Evans, D. Meier, S. Krohns, J.Appl. Phys. 129 (2021) 074101.

[71] J. Schultheiß,* E. Lysne, L. Puntigam, J. Schaab, E. Bourret, Z. Yan, S. Krohns, D. Meier, Nano Lett. 21 (2021) 9560.